The Cryosphere Discuss., 7, 5281–5306, 2013
www.the-cryosphere-discuss.net/7/5281/2013/
doi:10.5194/tcd-7-5281-2013

The Cryosphere Discussions
Open Access

Near-surface permeability in a supraglacial drainage basin on the Llewellyn glacier, Juneau Ice Field, British Columbia

L. Karlstrom[1], A. Zok[2], and M. Manga[2]

[1]Department of Geophysics, Stanford University, 397 Panama Mall, Stanford, CA 94305, USA
[2]Department of Earth and Planetary Science, 307 McCone Hall, University of California at Berkeley, Berkeley, CA 94720, USA

Received: 10 October 2013 – Accepted: 22 October 2013 – Published: 4 November 2013

Correspondence to: L. Karlstrom (leifk1@stanford.edu)

Published by Copernicus Publications on behalf of the European Geosciences Union.

Abstract

Supraglacial channel networks link time varying solar forcing and melt water routing on temperate glaciers. We present measurements of supraglacial channel spacing and network properties on the Juneau Icefield, subsurface water table height, and time variation of hydraulic characteristics including diurnal variability in water temperature. We combine these data with modeling of porous flow in weathered ice to infer near-surface permeability. Estimates are based on an observed phase lag between diurnal water temperature variations and discharge, and independently on measurement of water table surface elevation away from a stream. Both methods predict ice permeability on a 1–10 m scale in the range of 10^{-10}–10^{-11} m^2. These estimates are considerably smaller than common parameterizations of surface water flow on bare ice in the literature, as well as smaller than estimates of snowpack permeability. For supraglacial environments in which porosity/permeability creation in the subsurface is balanced by porous flow of melt water, our methods provide an estimate of microscale hydraulic properties from macroscale, remote observations of supraglacial channel spacing.

1 Introduction

In the ablation zone of glaciers and ice sheets, surface melt water channelizes and thermally erodes the icy substrate. This flowing melt water localizes to form supraglacial streams if melt production exceeds the transport capacity of near-surface ice, firn or snowpack. Supraglacial melt transport links surface melt to subglacial hydrologic systems through englacial drainage (Fountain and Walder, 1998), so temporal variations in the rate and volume of supraglacial melt water production has the potential to influence the basal environment and hence bulk ice movement (Bartholomaus et al., 2008; Colgan et al., 2011). Large amplitude englacial drainage events (Das et al., 2008) as well as diurnal (Shepherd et al., 2009) and seasonal (Palmer et al., 2011) variability in surface melting all influence large scale motion of ice masses.

TCD
7, 5281–5306, 2013

A critical parameter to both developing and sustaining streams is the permeability of near-surface ice that controls transport of meltwater into channels. Over bare and impermeable ice or in channels, flow timescales are commonly parameterized according to an effective friction parameter (Manning's equation, e.g., Arnold et al., 1998). However, in some settings there is also a layer of fractured, partially melted or otherwise weathered bare ice in the near surface through which porous flow of melt may occur. Because channelized flow moves quite rapidly (typical velocities $\sim 1\,\mathrm{m\,s^{-1}}$), subsurface porous flow if present will be the limiting factor for propagation of diurnal signals into the glacier. Permeability varies as a function of depth because melting attenuates with the decay of solar radiation in the subsurface and percolating melt water can refreeze (Pfeffer et al., 1991). It will also vary with altitude and season as surface snow transitions to bare ice down glacier (Braithwaite et al., 1994).

Ice permeability sets the transport efficiency of the supraglacial system, a quantity of interest in large-scale and short-time water budgets for glaciers and ice sheets (Rennermalm et al., 2013). Measurements of firn and weathered ice permeability have been conducted on 0.1–1 m scale samples (e.g., Fountain, 1989; Albert et al., 2000). But because permeability is often a scale-dependent material property (e.g., Schulze-Makuch et al., 1999), larger scale measurements may provide better characterization of hydraulic transport relevant to supraglacial channels. Such measurements may also be more relevant for connecting permeability to porosity measurements taken on larger (100–1000 m) scale (e.g., Morris and Wingham, 2011; Brown et al., 2012). Intermediate (1–100 m) scale permeability relevant for supraglacial stream channel formation and spacing (e.g., Marston, 1983) is not well constrained.

Here we present measurements of supraglacial stream channel networks high in the ablation zone of the Llewellyn glacier on the Juneau Icefield, British Columbia, over four days in August 2010. These measurements reveal how near-surface permeability is expressed in the distribution and time variation of melt transport. We measure time-varying discharge, water temperature and geometrical properties of a supraglacial drainage basin including channel aspect ratio, channel spacing and the height of the

TCD
7, 5281–5306, 2013

subsurface water table away from channels. We develop two methods to infer near-surface permeability, on a length scale of 1–10 m that is relevant to channel development. One method is based on modeling the elevation of the subsurface water table that extends perpendicular to channels, while the other uses a phase shift observed between stream water temperature and discharge to infer a subsurface transport lag. Both methods result in similar estimates for permeability of near-surface ice. We end by illustrating how these methods could be extended via remote sensing observations to large scale supraglacial drainage networks such as those on the West Greenland Ice Sheet.

2 Site summary and methods

The Llewellyn glacier drains the Juneau Icefield, on the Eastern side of the North American Continental Divide (Fig. 1a). Because of the local rain shadow and relatively high elevation (1300 m), the primary input to the supraglacial hydrologic network at this site is locally produced meltwater rather than rain. Average yearly rainfall in Atlin, BC (60 km East and 450 m lower that the Lewellyn site) is 0.192 m yr^{-1} (http://www.theweathernetwork.com). Our study site is a drainage basin near the Equilibrium Line Altitude near a medial moraine (Fig. 1b), exhibiting supraglacial channels that draw water from a layer of weathered, partially melted surface ice. Localization of melt water and thermal erosion causes supraglacial channels to form (Fig. 1c) where the gradient is low. Because of rapid glacier surface melting (several cm day^{-1}) channels in this environment form and become abandoned on day- to several day timescales, creating a hummocky glacier surface topography in the upper parts of the drainage basin that reflects competition between localized erosion by streams and large scale surface lowering.

We observed supraglacial streams during four consecutive days in August 2010. During this time we monitored one stream continuously, measuring water temperature, stream discharge and meteorological data. Surveying of stream network properties and

TCD
7, 5281–5306, 2013

glacier features such as fractures was accomplished with a combination of measuring tape and laser range finder (TruPulse 200B) with ~ 1 cm accuracy. Stream profiles were conducted using a Trimble R3 geodetic GPS unit (L1 band) in kinematic survey mode. Kinematic survey positions are accurate to 1 cm in the horizontal and 2 cm vertically.

Stream discharge was obtained using a Sontek Flowtracker handheld Acoustic Doppler Velocimeter to measure mean velocity (errors on these measurements typically ~ 0.1 $m s^{-1}$), and measuring tape for mean width and depth. All streams surveyed in this study were > 0.05 m deep at peak discharge. Melt rate at both sites was measured by observing bulk ice lowering around ice screws inserted perpendicular to the glacier surface. Water temperatures were monitored with HOBO loggers at both sites, although the ~ 0.5 °C resolution of these loggers is too coarse for sub-degree variation, and it was found that solar radiation highly biased even loggers covered with a reflective coating.

For more precise temperature measurements, we installed a Distributed Temperature Sensor (DTS) to obtain time series of stream water temperature. The DTS instrument is a cable thermometer that operates by firing short laser pulses down a length of fiber optic cable with a sensor measuring and integrating the spectrum of backscattered light. Light scattered by electrons in low-energy states returns to the detector slightly redshifted (Stokes scattering), while light scattered by electrons in high-energy states returns slightly blueshifted (anti-Stokes scattering). The temperature of a particular length of cable can be inferred from the amplitude ratio of the Stokes/anti-Stokes signals (Tyler et al., 2009) integrated over a specified time period.

Attenuation mechanisms within the cable itself are generally frequency dependent, so laser pulses are sent through the cable in both directions to allow the effects of differential attenuation to be measured and corrected for. To reduce the effects of instrument drift during a long deployment, calibration was performed continuously by comparing temperature measurements of an icewater bath (mixed by a motorized fish tank propeller) using both the DTS and a PT100 thermistor. 10 m of cable was placed in the ice bath. The instrument settings used allow temperature, location, and time to be resolved

TCD
7, 5281–5306, 2013

within 0.05 °C, 1 m, and 30 min respectively. Here we average measurements over the length of submerged (white colored) cable to get mean stream water temperature as a function of time. We ensure that during the day the cable is submerged in several centimeters of water to control for the effect of radiative cable heating by solar radiation. At night some cable is exposed, but the effects of radiation are then at a minimum, and it is easy to distinguish sections of cable exposed to the air by their higher temperatures.

Samples for stable isotopes of water $\delta^{18}O$ and $\delta^{2}H$ were collected at each site to characterize the bulk composition of stream water vs. glacier ice (taken in the stream headwaters near a bank). Care was taken during sampling to ensure no headspace air. Samples were analyzed with an isotope ratio mass spectrometer, with results reported in the conventional delta notation as per mil deviations from V-SMOW. Instrumental error in measurements is ~ 0.1 ‰ for O and ~ 0.5 ‰ for H isotopes.

Subsurface water table measurements were conducted through coring of near surface ice. Several 20–25 cm deep cores were taken in a straight line perpendicular to a stream at midday on a cloudless day, using a ~ 5 cm diameter pipe with a serrated end to facilitate coring.

Finally, we installed an eKo meteorological station that measured continuous time-series of wind speed and direction, net solar radiation, air temperature and relative humidity in the drainage basin. Meteorological measurements were carried out every 30 s for ~ 2 days, although instrument malfunction during the time period of DTS temperature measurements prevented complete overlap in datasets. We use daily averages of these data in what follows. For the period of our observation we take representative temperature of 7.8 °C, relative humidity 78 %, and wind speed 8.8 m s^{-1}.

3 Results

Coarse survey of the study supraglacial drainage basin (Fig. 1b, approximate area 0.07–0.08 km^2) reveals ubiquitous small streams with average daytime discharge of ~ 0.1 m^3 s^{-1}. A close coupling of melting to solar forcing (e.g., Marston, 1983) means

TCD
7, 5281–5306, 2013

that discharge at this site is strongly diurnal. Channel density decreases downstream (Fig. 2a), and streams high in the catchment exhibit close, regular spacing. Channel width to depth remains roughly constant throughout the drainage basin (Fig. 2b), consistent with the observation that the range in discharge is small. Hydraulic geometry of supraglacial streams does seem to vary as a function of discharge in general (Knighton, 1981). Abandoned channels are more common towards the top of the catchment compared to the bottom (Fig. 2c), indicative of active channel rearrangement. Streams combine downstream, and all eventually empty into a small number of fractures and moulins near a medial morraine that bounds our site. The underlying ice is relatively fracture free, so streams do not exhibit structural control. Discharge thus increases with distance downstream except where water drains into moulins.

We survey one stream in detail, choosing a reach with slope of 0.05 and of typical size for the area and performing a kinematic GPS survey along one bank of the stream (profile in Fig. 3a). Daily peak discharge of this stream is $0.13\,m^3\,s^{-1}$, characteristic channel width was 20–30 cm with depth of 5–8 cm. The upstream end of this channel is near the onset of channelization, and many small rivulets diverge upstream of this reach. The downstream end is an abrupt slope break near a medial moraine. Sinuosity (along-stream distance divided by straight line distance) for this stretch is 1.32, and local increases in slope appear to correlate with local increases in sinuosity (Ferguson, 1973).

The spectrum of sinuosity in this channel may be further quantified by expressing the GPS profile in terms of along-stream coordinates (θ, d) where θ is an angle from horizontal and d is a downstream distance increment (set by the number of points in each GPS survey – roughly 1 m for the stream in question). We then apply a wavelet transform to this channel profile using a Morlet mother wavelet (Mallat, 1999) (code courtesy of J. Taylor Perron). The results are shown in Fig. 3b, where solid contours are the periods that appear significant at the 95 % level compared to red noise. The black contour is the cone of influence for the transform. Anything below this line should be disregarded as insignificant.

TCD
7, 5281–5306, 2013

We see that lengthscales in the range of 4–16 m characterize the majority of the Llewellyn channel analyzed, with some suggestion of a (bimodal) longer wavelength superimposed, perhaps reflecting bed topography. The smaller wavelengths correspond to spacing between channels as shown by our coarse channel network survey (Fig. 2), reflecting a network dominated by the creation and abandonment of channels with no exogenic structural influence. Wavelengths measured here are also consistent with general scaling between meandering and channel width (meander wavelength = $8.014 \pm 0.517 \times$ channel width over three orders of magnitude in channel width; Karlstrom et al., 2013). This observation is also consistent with the inference by Karlstrom et al. (2013) that endogenic stream sinuosity occurs via a competition between localized thermal erosion in channels and broad scale lowering of the glacier surface.

3.1 Permeability of near-surface ice, Method 1

To estimate near-surface permeability, we utilize two indirect methods. The first method uses measurements of water table elevation in near surface ice perpendicular to a stream high in the drainage basin to infer transport. Porous subsurface ice is a thin unconfined aquifer above a less permeable ice layer, in which melt water flows down hydraulic gradients to streams. Because production of melt is strongly diurnal, the height of the aquifer varies in time and we use water table measurements along with a model of melt forcing to infer ice permeability. We assume that sublimation and evaporation are negligible compared with infiltration.

Picking a drainage divide between two channels that is roughly 2 m in length, in a transect away from one stream we take multiple cores to expose the water table (Fig. 4a). In the hole left behind from each core, the position of the water table is recorded in terms of its depth below the glacial surface. Cores revealed dry, porous ice (grain size 1–2 cm) near to the surface and fully saturated ice near the bottom (the water table). A wetting front extends ~ 1–2 cm above the water table, which exhibits an elevation of ~ 5 cm over a meter above the base stream level.

TCD
7, 5281–5306, 2013

Permeability may be estimated from these measurements by assuming spatially homogenous subsurface properties, then solving the equations for flow in an unconfined aquifer in 1-D. We solve the Boussinesq equation, obtained by combining Darcy's Law for porous flow with continuity of water, forced by influx due to melting N that is assumed constant over the domain x but time variable:

$$\frac{\partial h}{\partial t} = \kappa \frac{\partial^2 h^2}{\partial x^2} + \frac{N(t)}{\phi}, \tag{1}$$

where $\kappa = kg\rho/\mu\phi$ with k the permeability, ρ water density, μ water viscosity, g gravity and ϕ the porosity.

For two streams at the same elevation separated by a divide of length $2B$ (Fig. 4b), if N is constant in time the exact solution to Eq. (1) for water table height h is the Dupuit–Forchheimer ellipse (Bear, 1972)

$$h = \left[h_w^2 + \frac{N(2B - x)x}{\kappa} \right]^{1/2}, \tag{2}$$

where h_w is the (assumed equal) depth of the streams. The maximum elevation of the water table above the stream is $H_b = \sqrt{h_w^2 + NB^2/\kappa}$.

Ice screws inserted in the glacier surface provide estimates of melt rate during peak solar forcing of $\sim 1\,\mathrm{cm\,h^{-1}}$, which we might use as an estimate of N in Eq. (2). However, these influx rates are comparable to spatial subsurface water table changes from the stream, implying that the water surface height should not be considered steady in time. Measured water table elevations are small compared to the available porous layer in the ice (estimated to be 0.25–0.5 m in thickness) so a linearized version of the Boussinesq equation is appropriate, with $h' \ll h_0$:

$$\frac{\partial h'}{\partial t} = \kappa h_0 \frac{\partial^2 h'}{\partial x^2} + \frac{N(t)}{\phi}. \tag{3}$$

TCD
7, 5281–5306, 2013

We take N in the form

$$N(t) = n_0 e^{-(t-\mathrm{nint}(t))^2/\sigma^2}, \quad (4)$$

where t is simulation time in days (measured in days here for $N(t)$), nint refers to "next integer" and $\sigma = 6$ h, to model diurnal forcing with dominant 12 h melting period. We then solve this equation numerically with a Crank–Nicolson method, subject to boundary conditions that $h' = h_w$, the stream depth, at the channel outlet $x = 0$ and that $\partial h'/\partial x = 0$ at $x = B$, taken to be 1 m from our measurements. $h_w \sim 5$ cm in the channel nearest our measurements, $h_0 = 0.25$ m, and porosity we estimate as 10 % similar to some firn studies (Fountain, 1989). We estimate $n_0 \sim 1\,\mathrm{cm\,h^{-1}}$ although we consider this to be the most uncertain of parameter estimates. Other functional forms for melt rate Eq. (4) over a 12 h cycle (e.g., a sinusoid) do not affect the results.

Numerical results (Fig. 4c) show that water surface height varies diurnally. Because our measurements were taken near peak melting (1 p.m. LT), we use the maximum calculated water table height and perform a Newton–Raphson iteration to find the permeability that minimizes the difference between modeled and measured water table in a least squares sense (solid line in Fig. 4a), assuming $h_w = 0.05$ m, $B = 1$ m, $h_0 = 0.25$ m. For our measured $n_0 \sim 1\,\mathrm{cm\,h^{-1}}$ on the Llewellyn glacier we estimate $k \approx 1 \times 10^{-11}$ m^2, with $H_b - h_0 \sim 5$ cm the water table height above the stream, similar to estimates based on the static solution Eq. (2) with peak melting rate. In general there is a linear trade off between melt rate n_0 and permeability for this model (illustrated with the exact solution Eq. (2) in Fig. 7a).

3.2 Permeability of near-surface ice, Method 2

Our second method for estimating permeability uses time series measurements of stream flow and water temperature, in a section of stream ~ 100 m lower in the drainage basin than that surveying in Method 1. If surface ice is at the melting point, solar radiation during daylight hours will induce melting (and isotopic fractionation, reflected by

TCD
7, 5281–5306, 2013

shift of melt water composition between stream water and ice in Table 1). Once melting has occurred, additional solar radiation will heat water above the melting temperature. Thus we might expect diurnal variations of melt water temperature for sufficient solar heating, lagged by the thermal diffusion time for channels. For small streams of depth $D \sim 1\,\mathrm{cm}$ this timescale is $D^2/\kappa_d \sim 11\,\mathrm{min}$ for water thermal diffusivity of $\kappa_d = 1.5 \times 10^{-7}\,\mathrm{m\,s^{-2}}$. This is much shorter than the period of diurnal heating, so some temperature variability is to be expected in supraglacial streams. Solar heating of melt water will be thus an indirect tracer of melting surrounding ice, which also closely tracks downward radiation (Marston, 1983). We expect that slower porous transport of freshly melted ice to streams will then cause a lag between increases in water temperature and stream discharge that may be used to infer permeability of the porous flow region.

DTS Temperature measurements in the surveyed Llewellyn stream show differences in water temperature day to night. Raw DTS traces (Fig. 5a) resolve lengths of cable running over ice and cable submerged in water, with marked temperature differences between the two that decrease during nighttime when solar radiation does not heat the cable exposed directly to air. Because discharge varies diurnally, the length of cable submerged in the small channel varies as a function of time, with a fraction of the cable exposed to the air at night when discharge is low. This exposed cable is clearly distinguished in the temperature signal (grey vs. black curves at different times of day in Fig. 5a) and may be removed during post processing via thresholding. We therefore focus only on lengths of cable submerged in water, averaging over total submerged length to get a time series of average stream water temperature. A 24 h time series of DTS measurements during a cloudless day on the surveyed stream (peak discharge of $0.13\,\mathrm{m^3\,s^{-1}}$) show a smoothly varying water temperature between $\sim 0\,^{\circ}\mathrm{C}$ and $0.3\,^{\circ}\mathrm{C}$ (Fig. 5b), consistent with other measurements of supraglacial stream water temperature (Isenko et al., 2005).

While we do not measure discharge with the same time resolution as temperature, the length of cable submerged in the channel is a proxy for relative discharge because the instrumented reach has consistent (straight) geometry and the cable is well fixed

TCD
7, 5281–5306, 2013

in place with ice screws. We observe the expected lag between peak temperature and discharge (Fig. 6a). This lag as discussed above likely corresponds to the pore pressure diffusion timescale of supraglacial channels, if we assume that peak water temperature corresponds to peak melting (ice is at the melting point). By fitting sinusoids with a 24 h period to these timeseries, we determine a best fit lag of $\tau = 2.63$ h between peak temperature and peak discharge. We can use the observed lag between peak discharge and water temperature (Fig. 6a) to infer a permeability from our solution to Eq. (3), which also exhibits a lag between forcing and discharge (proportional to $\partial h'/\partial x$, Fig. 6b).

Using model parameters as with Method 1, a value of $k \approx 0.5\times10^{-11}$ m^2 produces the observed phase lag between melting and discharge at the stream. However because this channel is lower in the drainage basin than that for which we measure the water table, the distance between channels is larger (Fig. 2b), and therefore the recharge distance B is likely larger when solving Eq. (3). Calculated lag times are insensitive to the magnitude of melt influx n_0 because we are only concerned with the relative peak in discharge and n_0 is spatially homogeneous in our model. Fixing $n_0 = 1$ cm h^{-1} but varying B, all other parameters as used in the previous calculation, we find a range of permeabilities as a function of B that fits the observed time phase lag of 2.63 h (Fig. 7b). If we take $B = 10$ m as representative for the integrated upstream channels, we find $k = 8 \times 10^{-11}$ m^2.

4 Discussion and conclusions

We have estimated permeability of near-surface ice high in the ablation zone of the Llewellyn glacier, using two independent methods that link observed drainage network properties to near-surface glacial hydrology. Permeability inferred by measuring water table elevation away from a stream (Method 1) is consistent within an order of magnitude to permeability estimated from lag times between peak temperature and peak discharge (Method 2, Fig. 7). The permeability inferred from Method 2 is slightly larger,

TCD
7, 5281–5306, 2013

suggesting perhaps some scale dependence of permeability based the larger length scales of the estimate (~ 10 m vs. ~ 1 m based on channel spacing differences within the drainage basin, Fig. 2). Scale dependence in near-surface permeability is common (e.g., Schulze-Makuch et al., 1999), although our current data do not allow for further investigation of this matter. Larger permeability on a 10 m scale than a 1 m scale would occur if, for example, fractures began to exert an influence on infiltration at the larger scale.

The permeabilities inferred by our measurements are 1–2 orders of magnitude smaller than permeabilities of near surface snow and firn (e.g., Courville et al., 2010), values often employed for Darcy flow at the base of a snowpack or firn layer in the upper ablation zone (Arnold et al., 1998). Our measurements are, however, similar to ~ 0.1–0.3 m scale near-surface permeability measurements of sea ice at temperate latitudes (Kawamura et al., 2006).

The seasonal development of supraglacial stream networks reflects competition between surface melting, endogenic channelization instabilities and external control by underlying glacier structure. Supraglacial hydrology directly couples surface processes to solar forcing, so characterizing this system is important for understanding the response of glaciers and ice sheets to evolving surface energy balance. As the accumulation and retention of meltwater has considerable variability in large scale systems such as the Greenland ice sheet (e.g. Braithwaite et al., 1994; Rennermalm et al., 2013), field scale estimates of near-surface permeability may better inform models for surface runoff and energy balance (e.g., Bougamont and Bamber, 2005; Banwell et al., 2012a).

Many such models assume that friction-limited surface flow sets the transport rate of surface meltwater, for example into supraglacial lakes and moulins that then connect to the subglacial hydrological system. If flow is instead dominated by porous flow in weathered near-surface ice, these models will significantly under estimate the timescales of surface melt routing. Because the regime of supraglacial melt water transport may vary spatially and in time, it may be important to model the development and seasonal evo-

TCD
7, 5281–5306, 2013

lution of channel networks and supraglacial drainage basins to predict the large scale response of large ice masses to surface melting (Palmer et al., 2011).

As an illustration, we apply our methods to data from a study of West Greenland supraglacial drainage in August 2009 made by McGrath et al. (2010). These authors provide a survey of channels comprising one drainage basin, and measure a phase lag between daily maximum melt production averaged over the basin and stream discharge measured at a moulin that drains the basin. Typical stream velocities are 0.25–0.5 $\mathrm{m\,s^{-1}}$, ~ 5 orders of magnitude greater than likely Darcy velocities in the subsurface. Therefore, any phase lag between discharge and melting should be limited by transport of melt to streams. This will occur either through subsurface porous flow or via surface flow if the transport capacity of the subsurface is exceeded. We digitally measure via pixel counting the distance between 35 stream segments in Fig. 1 of McGrath et al. (2010), which yields a channel spacing of 18.0 ± 6.7 m high in the drainage basin. Taking half this distance as the typical recharge lengthscale B in our model estimates (Fig. 4), we can use the measured phase lag of 2.8 ± 4.2 h to estimate permeability of ice in this region as $k \approx 7 \times 10^{-11}$ $\mathrm{m^2}$. This is considerably smaller than permeabilities used in current models (Arnold et al., 1998), although we advocate caution and site specific calibration before directly applying our measurements on the Juneau Icefield to West Greenland.

Not all supraglacial environments exhibit a porous near-surface region that accommodates significant subsurface porous flow, particularly if melt rates or external water input rates are high. A near-surface aquifer of melt water is to be expected only where the creation of porosity/permeability (by melting or sublimation) is not outpaced by influx of melt water from surroundings. Still, a surface layer of porous and/or fractured ice is common, and in these settings the water table height will depend on a balance between time varying porosity creation and porous flow.

If macro scale characteristics of supraglacial drainage such as channel spacing generally reflect transport efficacy, our study provides a basis for remotely estimating permeability with models calibrated by field data. It suggests dependencies on the char-

TCD
7, 5281–5306, 2013

acteristic length scales of channels to complement other remote sensing techniques (e.g., Brown et al., 2012). By establishing a connection between near-surface ice permeability and channel spacing, we can connect microscale hydraulic characteristics of ablation zone surface ice to macroscale features that are observable in satellite imagery (e.g., Yang and Smith, 2013).

If calibrated and tested by field measurements, the models presented here could have application in the remote study of seasonal melt water routing evolution on large scales that are otherwise inaccessible to direct observation. In West Greenland, supraglacial lake occurrence, longevity and size covary with melt intensity (Liang et al., 2012). Similarly, controls on supraglacial stream occurrence and spacing such as near-surface permeability may be expected to vary seasonally and year to year. Because surface flow sets the timescale for supraglacial lake filling and subsequent draining (Hoffman et al., 2011; Banwell et al., 2012a, b), better constraints on field scale, near-surface permeability should help to better link surface mass balance with glacier and ice sheet movements in general.

Acknowledgements. We thank Eran Hood for logistical help and comments, NorthStar Trekking and the Juneau Icefield Research Program for logistical support, GSA and the UC Berkeley Behman fund for graduate student field work grants to L. Karlstrom, the Ramsden fund for support to A. Zok. We thank Scott Tyler and CTEMPs for a student grant to use DTS equipment. Ronnie Wentzel is acknowledged for GPS data, and Wenbo Yang performed isotopic analyses. We thank Johnny Sanders for glaciological field equipment.

References

Albert, M. R., Shultz, E. F., and Perron Jr., F. E.: Snow and firn permeability at Siple Dome, Antarctica, Ann. Glaciol., 31, 353–356, 2000. 5283

Arnold, N., Richards, K., Willis, I., and Sharp, M.: Initial results from a distributed, physically based model of glacier hydrology, Hydrol. Process., 12, 191–219, 1998. 5283, 5293, 5294

TCD
7, 5281–5306, 2013

Banwell, A., Arnold, N., Willis, I., Tedesco, M., and Alstrom, A.: Modeling supraglacial water routing and lake filling on the Greenland Ice Sheet, J. Geophys. Res., 117, F04012, doi:10.1029/2012JF002393, 2012a. 5293, 5295

Banwell, A., Willis, I., Arnold, N., Messerli, A., Rye, C., and Ahlstrom, A.: Calibration and validation of a high resolution surface mass balance model for Paakitsoq, west Greenland, J. Glaciol., 58, 1047–1062, 2012b. 5295

Bartholomaus, T., Anderson, R., and Anderson, S.: Response of glacier basal motion to transient water storage, Nat. Geosci., 1, 33–37, 2008. 5282

Bear, J.: Dynamics of Fluids in Porous Media, Dover Publications, New York, 1972. 5289

Bougamont, M. and Bamber, J. L.: A surface mass balance model for the Greenland Ice Sheet, J. Geophys. Res., 110, F04018, doi:10.1029/2005JF000348, 2005. 5293

Braithwaite, R. J., Laternser, M., and Pfeffer, W. T.: Variations of near-surface firn density in the lower accumulation area of the Greenland ice sheet, Pakitsoq, West Greenland, J. Glaciol., 40, 477–485, 1994. 5283, 5293

Brown, J., Bradford, J., Harper, J., Pfeffer, W., Humphrey, N., and Mosley-Thompson, E.: Georadar-derived estimates of firn density in the percolation zone, western Greenland ice sheet, J. Geophys. Res., 117, F01011, doi:10.1029/2011JF002089, 2012. 5283, 5295

Colgan, W., Rajaram, H., Anderson, R., Steffen, K., Phillips, T., Joughin, I., Zwally, H., and Arbalati, W.: The annual glaciohydrology cycle in the ablation zone of the Greenland ice sheet: Part 1. Hydrology model, J. Glaciol., 57, 697–709, 2011. 5282

Courville, Z., Horhold, M., Hopkins, M., and Albert, M.: Lattice–Boltzmann modeling of the air permeability of polar firn, J. Geophys. Res., 115, F04032, doi:10.1029/2009JF001549, 2010. 5293

Das, S. B., Joughin, I., Behn, M. D., Howat, I. M., King, M. A., Lizarralde, D., and Bhatia, M. P.: Fracture propoagation to the base of the Greenland Ice Sheet during supraglacial lake drainage, Science, 320, 5877, doi:10.1126/science.1153360, 2008. 5282

Ferguson, R. I.: Sinuosity of supraglacial streams, Geol. Soc. Am. Bull., 84, 251–256, 1973. 5287

Fountain, A. G.: The storage of water in, and hydraulic characteristics of, the firn of South Cascade Glacier, Washington State, USA, Ann. Glaciol., 13, 69–75, 1989. 5283, 5290

Fountain, A. G. and Walder, J. S.: Water flow through temperature glaciers, Rev. Geophys., 36, 299–328, 1998. 5282

TCD
7, 5281–5306, 2013

Hoffman, M., Catania, G., Neumann, T., Andrews, L., and Rumrill, J.: Links between acceleration, melting, and supraglacial lake drainage of the western Greenland Ice Sheet, J. Geophys. Res., 116, F04035, doi:10.1029/2010JF001934, 2011. 5295

Isenko, E., Narus, R., and Mavlyudov, B.: Water temperature in englacial and supraglacial channels: change along the flow and contribution to ice melting on the channel wall, Cold Reg. Sci. Technol., 42, 53–62, 2005. 5291

Karlstrom, L., Gajjar, P., and Manga, M.: Meander formation in supraglacial streams, J. Geophys. Res., 118, 1897–1907, doi:10.1002/jgrf.20135, 2013. 5288

Kawamura, T., Ishikawa, M., Takatsuka, T., Kojima, S., and Shirasawa, K.: Measurements of permeability of sea ice, in: Proceedings of the 18th IAHR International Symposium on Ice, 105–112, 2006. 5293

Knighton, A. D.: Channel form and flow characteristics of supraglacial streams, Austre Okstindbreen, Norway, Arct. Alp. Res., 13, 295–306, 1981. 5287

Liang, Y.-L., Colgan, W., Lv, Q., Steffen, K., Abdalati, W., Stroeve, J., Gallaher, D., and Bayou, N.: A decadel investigation of supraglacial lakes in West Greenland using a fully automatic detection and tracking algorithm, Remote Sens. Environ., 123, 127–138, 2012. 5295

Mallat, S.: A Wavelet Tour of Signal Processing, Academic Press, San Diego, 1999. 5287

Marston, R. A.: Supraglacial stream dynamics on the Juneau Icefield, Ann. Assoc. Am. Geogr., 73, 597–608, 1983. 5283, 5286, 5291

McGrath, D., Colgan, W., Steffen, K., Lauffenburger, P., and Balog, J.: Assessing the summer water budget of a moulin basin in the Sermeq Avannarleq ablation region, Greenland ice sheet, J. Glaciol., 56, 954–964, 2010. 5294

Morris, E. and Wingham, D.: The effect of fluctuations in surface density, accumulation and compaction on elevation change rates along the EGIG line, central Greenland, J. Glaciol., 57, 416–430, 2011. 5283

Palmer, S., Shepherd, A., Nienow, P., and Joughin, I.: Seasonal speedup of the Greenland Ice Sheet linked to routing of surface water, Earth Planet. Sc. Lett., 302, 423–428, 2011. 5282, 5294

Pfeffer, W., Meier, M., and Illanasekare, T.: Retention of Greenland runoff by refreezing: implications for projected future sea level change, J. Geophys. Res., 96, 22117–22124, 1991. 5283

TCD
7, 5281–5306, 2013

Rennermalm, A., Moustafa, S., Mioduszewski, J., Chu, V., Forster, R., Hagedorn, B., Harper, J., Mote, T., Robinson, D., Shuman, C., Smith, L., and Tedesco, M.: Understanding Greenland ice sheet hydrology using an integrated multi-scale approach, Environ. Res. Lett., 8, 015017, doi:10.1088/1748-9326/8/1/015017, 2013. 5283, 5293

Schulze-Makuch, S., Carlson, D., Cherkauer, D., and Malik, P.: Scale dependency of hydraulic conductivity in heterogeneous media, Ground Water, 37, 904–919, 1999. 5283, 5293

Shepherd, A., Hubbard, A., Niewnow, P., King, M., McMillan, M., and Joughin, I.: Greenland ice sheet motion coupled with daily melting in late summer, Geophys. Res. Lett., 36, L01501, doi:10.1029/2008GL035758, 2009. 5282

Tyler, S. W., Selker, J. S., Hausner, M. B., Hatch, C. E., Torgersen, T., Thodal, C. E., and Schladow, S. G.: Environmental temperature sensing using Raman spectra DTS fibre-optic methods, Water Resour. Res., 45, W00D23, doi:10.1029/2008WR007052, 2009. 5285

Yang, K. and Smith, L.: Supraglacial streams on the Greenland Ice Sheet delineated from combined spectral-shape information in high-resolution satellite imagery, IEEE T. Geosci. Remote, 10, 801–805, doi:10.1109/LGRS.2012.2224316, 2013. 5295

TCD
7, 5281–5306, 2013

Table 1. Oxygen and hydrogen isotopic composition of water samples from three different streams on the Llewellyn glacier, as well as ice near one stream and rain water in Juneau, AK, measured during the same time period. All measurements have units of ‰ deviation from V-SMOW.

Site	Sampling time	$\delta^{18}O$	$\delta^{2}H$
Llewellyn stream 1	4 August, 3.00 p.m.	−18.77	−143.27
Llewellyn stream 2	4 August, 3.00 p.m.	−18.87	−142.72
Llewellyn stream 3	4 August, 3.00 p.m.	−18.83	−142.05
Llewellyn ice near stream 3	4 August, 3.00 p.m.	−19.06	−145.07
Rain water in Juneau	31 July, 6.30 p.m.	−9.60	−70.02

TCD
7, 5281–5306, 2013

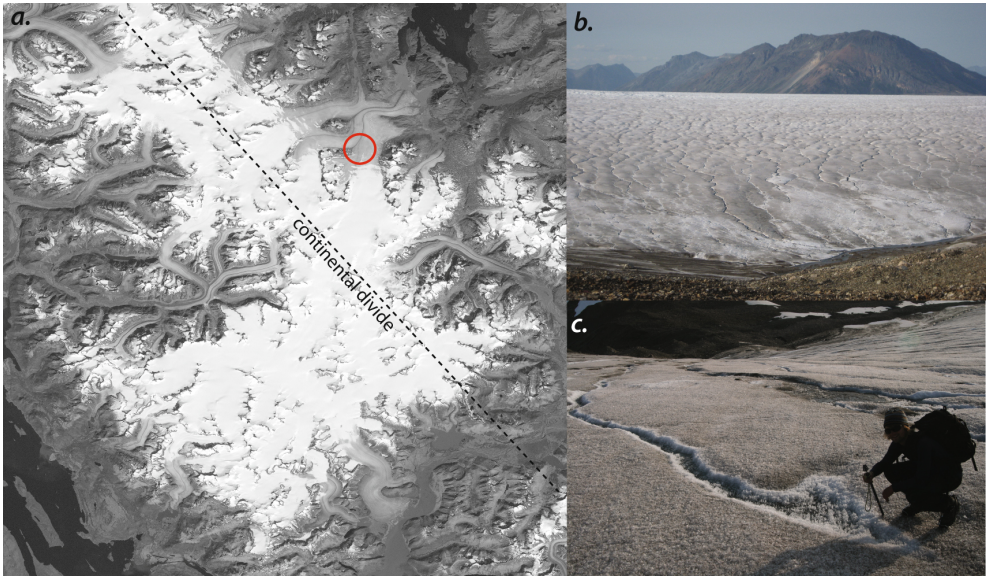

Fig. 1. (a) Regional map of Juneau Icefield, showing the Llewellyn glacier study site (solid red circle). Image courtesy Paul Illsley. **(b)** The supraglacial drainage basin studied here, photo taken from medial morraine. Note hummocky topography and closely spaced channels high in the basin, with more linear and widely spaced channels lower down. **(c)** Inception of a supraglacial channel high in the upper study drainage basin, with porous icy substrate surrounding.

TCD
7, 5281–5306, 2013

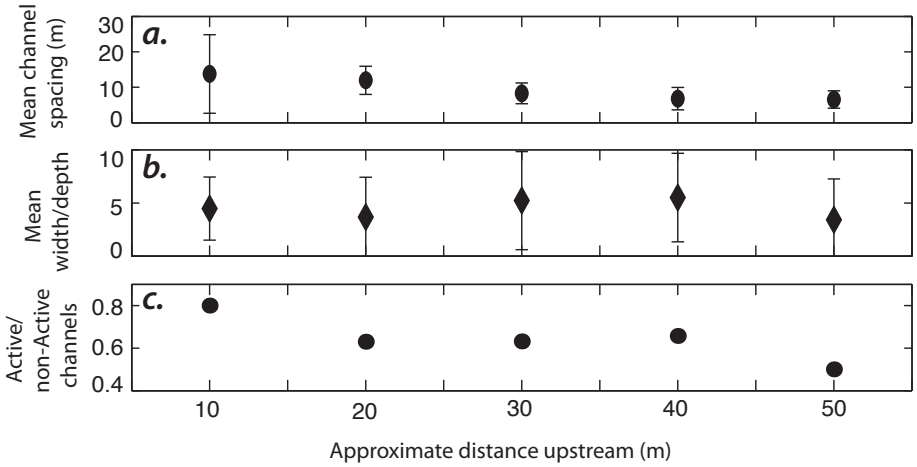

Fig. 2. Network characteristics of the Llewellyn drainage basin shown in Fig. 1b, higher numbers moving upstream. **(a)** Mean channel spacing (inverse of channel density) with standard deviation error bars. **(b)** Mean width to depth of active channels, with standard deviation. **(c)** Ratio of active to non-active (abandoned) channels.

TCD
7, 5281–5306, 2013

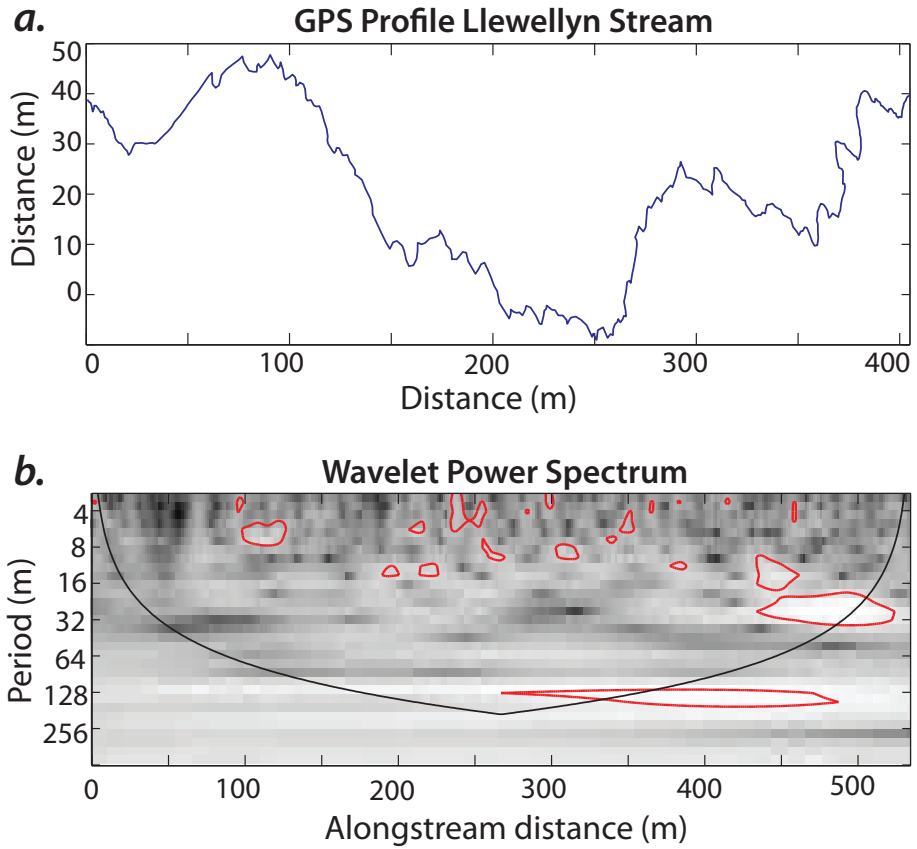

Fig. 3. (a) Kinematic GPS profile in map view of individual streams on the Llewellyn glacier. Stream flow is from right to left, and average slope is ~ 0.05. **(b)** Wavelet power spectra of the profile in **(a)**, with 95 % significance contours with respect to red noise (solid red lines) and the Morlet wavelet cone of influence for each survey. More details in text.

TCD
7, 5281–5306, 2013

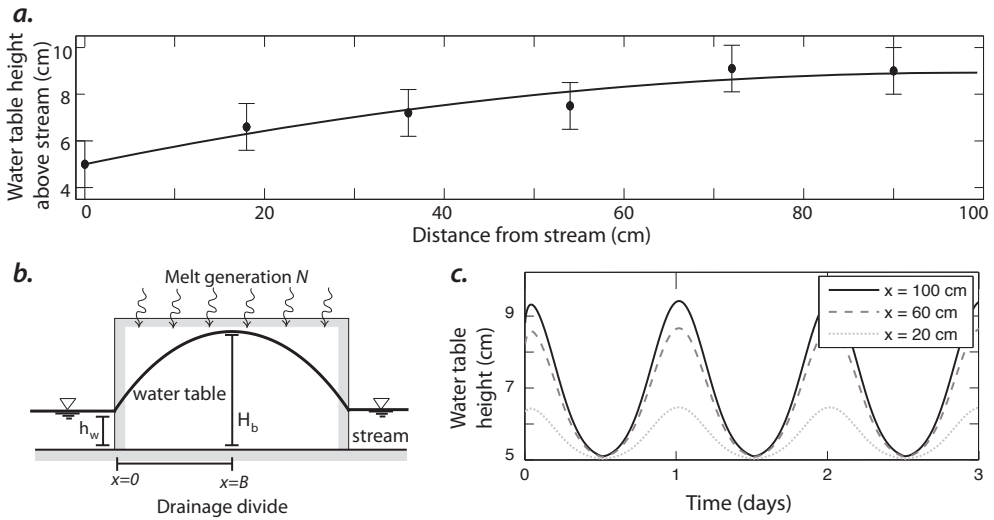

Fig. 4. (a) Water table height measurements as a function of distance away from a stream, with nonlinear fit of Eqs. (3) and (4), assuming $n_0 = 0.01\,\mathrm{m\,h^{-1}}$ and peak melting, $B = 1\,\mathrm{m}$, $h_w = 0.05\,\mathrm{m}$, $\phi = 10\,\%$ and $k = 1 \times 10^{-11}\,\mathrm{m^2}$. Error bars are 1 cm. **(b)** Sketch of the model problem and geometry, illustrating Dupuit–Forchheimer ellipse. **(c)**. Variation of water table height $h(x, t)$ from numerical solution to Eq. (3) parameters as in **(a)**. Curves plot points along the profile as a function of time.

TCD
7, 5281–5306, 2013

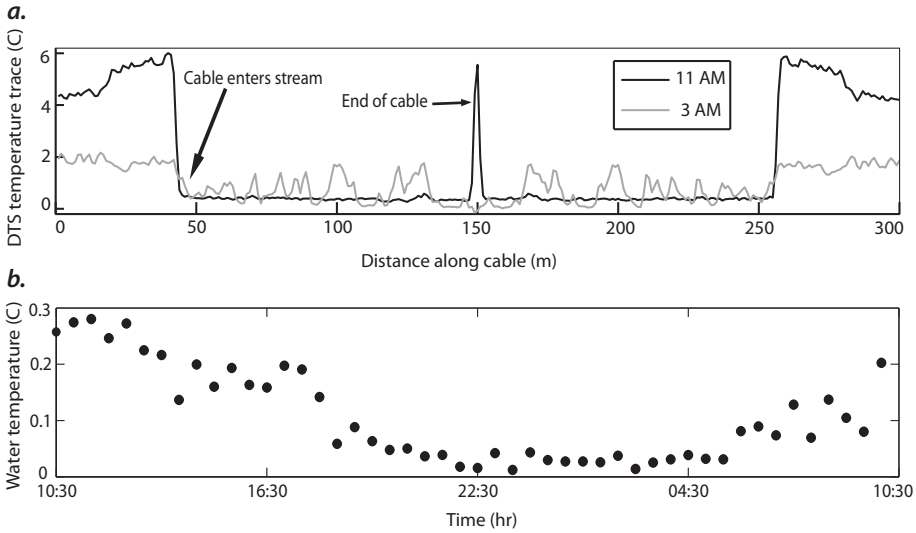

Fig. 5. (a) Unfiltered DTS temperature trace at 11 a.m. (black curve) and 3 a.m. (grey curve). The cable runs from the sensor to a water bath (not plotted), over glacier ice to the stream. The point of cable entry into the stream and end of cable (these are double-ended measurements, so trace is symmetric about midpoint) are labeled. **(b)** DTS timeseries over 24 h on a clear day, filtered spatially and averaged for water temperature. Each point is the average temperature along the submerged length of the cable.

TCD
7, 5281–5306, 2013

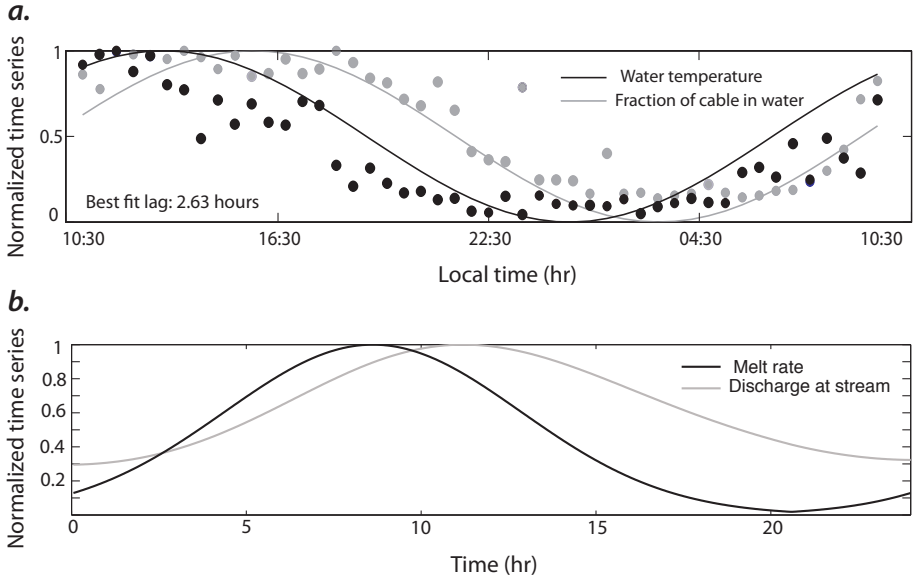

Fig. 6. (a) Lag between normalized timeseries of DTS temperature and fraction of cable in water (Fig. 5) with nonlinear fits of daily-periodic sinusoids. **(b)** Modeled time lag between discharge at channel outlet and melt input (assumed constant over the domain). Length of recharge is $B = 10$ m, all other parameters as in Fig. 4.

TCD
7, 5281–5306, 2013

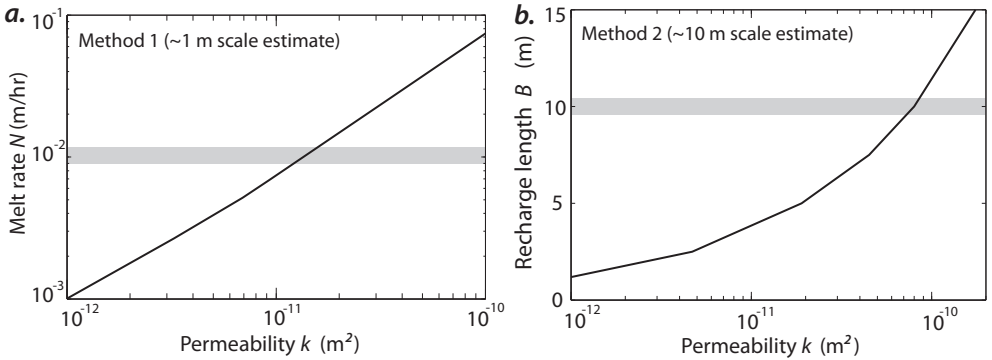

Fig. 7. Summary of permeability estimates from the two methods presented in the text. **(a)** Predicted permeability as a function of melt influx rate N from Eqn. (2)–(4) and Llewellyn glacier water table measurements. **(b)** Permeability estimated from matching the phase lag between discharge at stream and melt input (Fig. 6a) as a function of recharge lengthscale B. Estimates for melt rate **(a)** and recharge length **(b)** are shown with grey bars.

TCD
7, 5281–5306, 2013